HHS Public Access

Author manuscript

Sci Transl Med. Author manuscript; available in PMC 2019 December 03.

Published in final edited form as:

Sci Transl Med. 2018 September 05; 10(457): . doi:10.1126/scitranslmed.aat1662.

Hypercapnia increases airway smooth muscle contractility via caspase-7-mediated miR-133a-RhoA signaling

Masahiko Shigemura[1,2], **Emilia Lecuona**[1], **Martín Angulo**[3], **Tetsuya Homma**[4], **Diego A. Rodríguez**[5], **Francisco J. Gonzalez-Gonzalez**[1], **Lynn C. Welch**[1], **Luciano Amarelle**[1,3], **Seok-Jo Kim**[1,6], **Naftali Kaminski**[7], **G. R. Scott Budinger**[1], **Julian Solway**[8], **Jacob I. Sznajder**[1,*]

[1]Division of Pulmonary and Critical Care Medicine, Northwestern University, Chicago, IL 60611, USA.

[2]First Department of Medicine, Hokkaido University School of Medicine, Sapporo, Japan.

[3]Pathophysiology Department, School of Medicine, Universidad de la República, Montevideo, Uruguay.

[4]Division of Allergology and Respiratory Medicine, Department of Internal Medicine, Showa University School of Medicine, Tokyo, Japan.

[5]Pulmonology Department, Hospital del Mar, Institut Hospital del Mar d'Investigacions Mèdiques, Universitat Pompeu Fabra, Centro de Investigación Biomédica en Red de Enfermedades Respiratorias (CIBERES), ISCiii, Barcelona, Spain

[6]Department of Medicine, Division of Pulmonary and Critical Care Medicine, Jesse Brown Veterans Affairs Medical Center, Chicago, IL 60612, USA.

*Corresponding author j-sznajder@northwestern.edu.

Author contributions: M.S., E.L., and J.I.S. contributed to all study design and data interpretation and wrote the manuscript. M.A. and N.K. performed the microarray experiments. M.S. and M.A. analyzed the data. M.S., T.H., and D.A.R designed the COPD cohort study and analyzed the data of respiratory/airway resistance in COPD patients. M.S., F.J.G.-G., L.C.W., L.A., and J.S. designed and conducted the animal experiments and analyzed the data. G.R.S.B., S.-J.K., and J.S. interpreted all the data and wrote the paper. J.I.S. and G.R.S.B. provided the funding. S.-J.K. and G.R.S.B. provided the resources.

Competing interests: The authors declare that they have no competing financial interests.

SUPPLEMENTARY MATERIALS

www.sciencetranslationalmedicine.org/cgi/content/full/10/457/eaat1662/DC1

Materials and Methods

Fig. S1. Normoxic hypercapnia alters gene expression in mouse lung.

Fig. S2. Quantification of Mef2D-positive cell in mouse ASM cells.

Fig. S3. High CO_2 causes caspase-dependent cleavage of Mef2D protein, resulting in down-regulation of miR-133a, but does not induce apoptosis in mouse ASM cells.

Fig. S4. Acute hypercapnia causes ASM relaxation due to hypercapnia-associated acidosis.

Fig. S5. Central respiratory resistance in WT and Caspase-7-null mice.

Fig. S6. RhoA protein abundance and Mlc phosphorylation in mouse primary alveolar type II cells.

Fig. S7. Quantification of cleaved Mef2D in ASM cells from Caspase-7-null mice.

Fig. S8. Schematic of nonapoptotic role of Caspase-7 in ASM contractility during hypercapnia.

Fig. S9. Same signaling pathways activated in mouse ASM cells when exposed to similar pCO_2 values to the COPD patients.

Table S1. Processed data from mRNA and miR microarray analysis of lungs isolated from C57BL/6J mice exposed to normoxic hypercapnia or room air for 3 or 7 days (Excel file).

Table S2. Primary data (Excel file).

References (42, 43)

Data and materials availability: All the data are included in the paper or in the Supplementary Materials.

[7]Department of Internal Medicine, Section of Pulmonary, Critical Care, and Sleep Medicine, Yale School of Medicine, New Haven, CT 06520, USA.

[8]Department of Medicine, University of Chicago, Chicago, IL 60637, USA.

Abstract

The elevation of carbon dioxide (CO_2) in tissues and the bloodstream (hypercapnia) occurs in patients with severe lung diseases, including chronic obstructive pulmonary disease (COPD). Whereas hypercapnia has been recognized as a marker of COPD severity, a role for hypercapnia in disease pathogenesis remains unclear. We provide evidence that CO_2 acts as a signaling molecule in mouse and human airway smooth muscle cells. High CO_2 activated calcium-calpain signaling and consequent smooth muscle cell contraction in mouse airway smooth muscle cells. The signaling was mediated by caspase-7-induced down-regulation of the microRNA-133a (miR-133a) and consequent up-regulation of Ras homolog family member A and myosin light-chain phosphorylation. Exposure of wild-type, but not caspase-7-null, mice to hypercapnia increased airway contraction and resistance. Deletion of the ***Caspase-7*** gene prevented hypercapnia-induced airway contractility, which was restored by lentiviral transfection of a miR-133a antagonist. In a cohort of patients with severe COPD, hypercapnic patients had higher airway resistance, which improved after correction of hypercapnia. Our data suggest a specific molecular mechanism by which the development of hypercapnia may drive COPD pathogenesis and progression.

INTRODUCTION

Gaseous molecules such as oxygen (O_2), nitric oxide, and carbon dioxide (CO_2) are sensed by cells and activate specific intracellular signaling pathways (1–3). Cellular responses to CO_2 were thought to be a consequence of acidosis because of the rapid conversion of CO_2 in solution into carbonic acid, which leads to bicarbonate and hydrogen ion formation. However, recent studies suggest that high concentration of CO_2 acts as a signaling molecule in the lung, activating signaling transduction pathways (4) and altering transcription factor activity (5) and microRNA (miR) expression (6).

Hypercapnia, defined as an elevation in the arterial CO_2 tension, is a complication of inadequate alveolar gas exchange in patients with severe acute and chronic lung diseases including chronic obstructive pulmonary disease (COPD) (3, 7). About 16 million individuals in the United States have COPD, which is currently the third leading cause of death, and the rates of mortality attributable to COPD continue to rise (8, 9). Persistent hypercapnia is associated with increased mortality among COPD patients (7). The recent discovery that treating hypercapnic COPD patients with noninvasive ventilation reduced mortality (10, 11) raised the possibility that hypercapnia itself might be involved in the disease pathogenesis and progression.

We hypothesized that CO_2 elevation activates signaling pathways in the airways that results in pathological changes in lung function. Here, we provide evidence that high CO_2 induces airway smooth muscle (ASM) contractility via Caspase-7-mediated miR-133a-Ras homolog family member A (RhoA) axis signaling in rodents. Our data suggest that development of hypercapnia worsens airway constriction and may limit ventilation to poorly functioning

lung units by inducing excess constriction of the airways, setting up a feedback loop that could culminate in respiratory failure.

RESULTS

High CO_2 increases ASM cell contractility via miR-133a-mediated RhoA signaling

To elucidate the effects of hypercapnia on airway cells, we first performed mRNA and miR microarray analysis of lungs isolated from C57BL/6J mice exposed to normoxic hypercapnia (10% CO_2 and 21% O_2) or room air for 3 or 7 days (fig. S1, A and B). Exposure to hypercapnia altered gene expression in the lung. We found 1017 and 2959 genes that were differentially expressed in mice exposed to hypercapnia for 3 or 7 days, respectively (table S1). MetaCore pathway analysis revealed that the most enriched pathway was “ASM contraction in asthma” (fig. S1C). To identify potential-enriched ASM contraction pathways, MetaCore network analysis that combined both mRNA and miRNA microarray data obtained from the lungs of mice exposed to hypercapnia was performed and suggested changes in the “miR-133a-related RhoA/myosin light-chain (Mlc) phosphatase-Mlc” pathway (fig. S1D).

The microarray data suggested that hypercapnia may alter airway contractility. To test this hypothesis, we measured acetylcholine (ACh)-induced cell contraction in primary mouse ASM cells incubated with normal CO_2 range (30 to 40 mmHg = 5%) or hypercapnic (60 to 80 mmHg = 10% or ~120 mmHg = 20% CO_2) and normoxic conditions with control of the extracellular pH. We found that ASM cells exhibited increased ACh-induced cell contraction dependent on CO_2 dose and exposure time (Fig. 1A). The cell contraction was independent of metabolic acidosis (Fig. 1A).

ASM contraction is effected through actin-myosin cross-bridge cycling, which is regulated by phosphorylation of the 20-kD regulatory MLC (12, 13). The RhoA-Rho-associated kinase (ROCK) signaling pathway induces phosphorylation and inactivation of MLC phosphatase and thus supports MLC phosphorylation and contractility of smooth muscle (12, 13).

To determine whether high CO_2 enhances Mlc phosphorylation through the RhoA-ROCK signaling pathway, we analyzed RhoA protein expression and Mlc phosphorylation in mouse ASM cells exposed to high (20%) CO_2. High CO_2 exposure for 2 or 7 days caused up-regulation of RhoA protein (Fig. 1B). Moreover, the increased Mlc phosphorylation and ASM cell contraction after 20% CO_2 exposure were prevented by preincubation with the ROCK inhibitor Y-27632 in mouse ASM cells (Fig. 1, C and D). One of the mechanisms recently recognized to increase RhoA protein expression is the down-regulation of miR-133a (14). We found that high CO_2 caused a time-dependent decrease in miR-133a expression in mouse ASM cells (Fig. 1E).

To determine whether the increased expression of RhoA protein by high CO_2 was due to the decrease in miR-133a expression, we transfected mouse ASM cells with mimic miR-133a before 20% CO_2 exposure and found that the up-regulation of RhoA protein in high CO_2 conditions was prevented in these cells (Fig. 1F). Moreover, we found an up-regulation of

RhoA protein in mouse ASM cells transfected with a miR-133a antagonist (antagomiR-133a) in normocapnic conditions (Fig. 1G).

To confirm a role for miR-133a in the high CO_2-induced ASM cell contractility, we overexpressed miR-133 in mouse ASM cells by lentiviral infection and found that the overexpression of miR-133 prevented the ACh-induced cell contraction observed in the cells exposed to 20% CO_2 (Fig. 1H). Collectively, our data suggest that high CO_2 reduces miR-133a abundance, thereby increasing RhoA protein expression, Mlc phosphorylation, and consequent ASM cell contraction. We also confirmed that high CO_2 increased ACh-induced cell contraction in human ASM cells (Fig. 2A), which was prevented by either Y-27632 (Fig. 2B) or lentiviral overexpression of miR-133 (Fig. 2C).

High CO_2 induces Caspase-7-dependent cleavage of myocyte-specific enhancer factor 2D and miR-133a down-regulation

Analysis of transcription factor binding sites for the miR-133a promoter using the transcription factor database (TRANSFAC, geneXplain) predicted myocyte-specific enhancer factor 2D (Mef2D) and Yin Yang 1 (Yy1) as candidates to bind the promoter of miR-133a in mouse lung (Fig. 3A). Therefore, we evaluated miR-133a expression in mouse ASM cells transfected with small interfering RNAs (siRNAs) for *Mef2d* or *Yy1* in normoxic conditions and found that the *Mef2d* siRNA caused down-regulation of miR-133a and up-regulation of RhoA protein, whereas the *Yy1* siRNA did not affect miR-133 expression (Fig. 3, B and C), suggesting that Mef2D was likely involved in the modulation of miR-133a in mouse ASM cells. Immunocytochemical analysis revealed that Mef2D was almost exclusively localized to the cell nucleus and that the number of Mef2D-positive cells was decreased in high CO_2 conditions (Fig. 3D and fig. S2). Western blot analysis revealed that Mef2D protein abundance was decreased in the nuclear fraction from mouse ASM cells exposed to high CO_2 conditions (Fig. 3E). The decreased expression of Mef2D protein resulted in less Mef2D bound to the miR-133a promoter in mouse ASM cells exposed to high CO_2 conditions (Fig. 3F).

To further explore the mechanism mediating Mef2D protein expression decreased by high CO_2, we examined *Mef2d* mRNA expression in mouse ASM cells exposed to high CO_2 conditions and found no differences between normocapnic and high CO_2 conditions (fig. S3A). We observed Mef2D fragments in the nuclear fractions in mouse ASM cells exposed to high CO_2 (Fig. 3E), suggesting Mef2D protein fragmentation. As a direct cleavage of MEF2D by caspase-7 has been shown (15), we used a nonselective caspase inhibitor, Z-VAD-FMK, to assess whether caspases were involved in the cleavage of Mef2D. Preincubation with Z-VAD-FMK prevented the fragmentation of Mef2D and rescued the down-regulation of miR-133a in high CO_2 conditions (fig. S3, B and C). To identify the specific caspase that cleaves Mef2D in high CO_2 conditions, we examined cleavage of Caspase-3, Caspase-7, Caspase-8, and Caspase-9 in mouse ASM cells exposed to high CO_2 and found that only Caspase-7 was cleaved (Fig. 3G and fig. S3, D to G). The cleavage of Caspase-7 was not associated with procaspase-7 expression (Fig. 3G). We did not observe increases in cleavage of poly(adenosine 5′-diphosphate-ribose) polymerase (PARP), DNA fragmentation, or positive terminal deoxynucleotidyl transferase-mediated deoxyuridine

triphosphate nick end labeling (TUNEL) staining in mouse ASM cells exposed to high CO_2 conditions (fig. S3, H to J), suggesting that high CO_2 does not cause cell apoptosis. To determine a role for Caspase-7 in high CO_2-induced Mef2D fragmentation, we used *Caspase-7* siRNA to silence *Caspase-7* and showed that the silencing prevented the formation of the Mef2D fragments and rescued the down-regulation of miR-133a in mouse ASM cells exposed to high CO_2 conditions (Fig. 3, H and I). Site-directed mutagenesis was performed to identify and evaluate Caspase-7 cleavage site of Mef2D. Mutation of residue 478 of Mef2D from aspartate to alanine also prevented the formation of the Mef2D fragments and rescued the down-regulation of miR-133a in high CO_2 conditions (Fig. 3, J to L). Collectively, our data suggest that high CO_2 activates Caspase-7, which, via a noncanonical pathway, cleaves Mef2D, thereby reducing miR-133a expression. Consistently with the data from mouse ASM cells, high CO_2 induced CASPASE-7-dependent cleavage of MEF2D in human ASM cells (Fig. 4A) with no changes of procaspase-7 expression (Fig. 4B).

High CO_2 activates calcium-calpain signaling, leading to Caspase-7 activation

Calpains, Ca^{2+}-dependent cysteine proteases, are known to modulate caspase activity via direct cleavage (16, 17). To assess the relationship between calpains and Caspase-7 in high CO_2 conditions, we monitored the activity of calpains in mouse ASM cells exposed to 20% CO_2. We found that the activity of calpains was tightly regulated and peaked at 6 hours of high CO_2 exposure (Fig. 5A). However, this increased activity was not due to increased abundance of major calpains, Calpain-1 and Calpain-2 (Fig. 5B). Recombinant caspase-7 has been reported to be directly cleaved by calpain-1 within the large subunit of caspase-7 to produce two subunits of 18.5 and 17.2 kDa, which are smaller than the 20-kDa subunit produced by caspase-3 cleavage (17). We show that *Calpain-1* siRNA, but not *Calpain-2* siRNA, prevented the high CO_2-induced Caspase-7 cleavage (Fig. 5C), suggesting intracellular Ca^{2+}-dependent cleavage of Caspase-7 via Calpain-1. Hypercapnia has been reported to lead to an increase in intracellular Ca^{2+} in alveolar epithelial cells (4, 18). We found that high CO_2 conditions increased intracellular Ca^{2+} in mouse ASM cells (Fig. 5D). ASM cells exposed to high CO_2 conditions and control cells had similar increased intracellular Ca^{2+} in response to ACh. However, high CO_2-exposed cells had an increased basal Ca^{2+} concentration as compared to control cells (Fig. 5E), suggesting that the basal increase in intracellular Ca^{2+} is important for CO_2, but not ACh, response.

We examined whether intracellular Ca^{2+} plays a role in Calpain-1 activation in mouse ASM cells exposed to high CO_2 conditions and found that a cell-permeant chelator, 1, 2-bis(2-aminophenoxy) ethane-*N, N, N′, N′*, -tetraacetic acid-acetoxymethyl ester (BAPTA-AM), prevented the increase in calpain activity (Fig. 5F). Together, our data suggest that high CO_2 increases intracellular Ca^{2+}, activating Calpain-1, which cleaves Caspase-7.

Chronic hypercapnia induces airway contractility, which is prevented in Caspase-7-null mice

The effects of hypercapnia on the airways and ASM have been controversial. There are reports attesting that hypercapnia causes airway relaxation (19, 20) or increased airway contractility (21, 22). We found that acute (1-hour exposure) hypercapnia caused modest

ASM relaxation due to the associated acidosis (fig. S4). However, prolonged hypercapnia, when the pH returns toward normal values, causes ASM cell contraction.

To translate the in vitro observations in an animal model, we exposed C57BL/6J WT mice to normoxic hypercapnia (10% CO_2 and 21% O_2) or room air conditions for up to 21 days and observed higher ACh-induced airway contraction in precision-cut lung slices (PCLSs) from mice exposed to hypercapnia (Fig. 6A). Airway resistance both before (basal tone) and after methacholine challenge in hypercapnia-exposed mice was also significantly increased on day 21 (Fig. 6B and fig. S5). Expression of miR-133a in the left main bronchial rings was significantly decreased in the hypercapnia-exposed mice (Fig. 6C). RhoA protein abundance and Mlc phosphorylation were significantly increased in lungs from the hypercapnia-exposed mice as compared to room air-exposed mice (Fig. 6D), with no differences observed in alveolar type II cells isolated from the lungs (fig. S6), suggesting that the pathway is not stimulated in the alveolar epithelium. The increased airway contraction and resistance, as well as miR-133a and RhoA protein expression and Mlc phosphorylation in the mice exposed to hypercapnia, were not observed in Caspase-7-null mice (Fig. 6, A to D) but were observed again in Caspase-7-null mice treated with antagomiR-133a by lentiviral infection (Fig. 6, A, C, and D). ASM cells isolated from Caspase-7-null mice and exposed to high CO_2 conditions had an increase in intracellular Ca^{2+} and calpain activation (upstream of high CO_2-induced events; Fig. 6, E and F) but did not exhibit the downstream effects of high CO_2 (cleavage of Mef2D, down-regulation of miR-133a, up-regulation of RhoA protein, and Mlc phosphorylation; Fig. 6, G to I, and fig. S7). Moreover, the ASM cells from mice lacking Caspase-7 had similar contractile responses to ACh in comparison with ASM cells from WT mice during normocapnia and did not show the increased contractility after a 2-day exposure to high CO_2 observed in WT cells (Fig. 6, J and K). Collectively, these data suggest that hypercapnia increases ASM contractility via a specific mechanism involving the nonapoptotic function of Caspase-7 (fig. S8).

Airway/respiratory resistance is increased in hypercapnic patients with COPD

Aiming to determine whether hypercapnia can induce broncho-constriction in humans, we measured airway or respiratory resistance by plethysmographic assessment or impulse oscillometry (IOS) in two cohorts of stable patients with chronic COPD. In both cohorts, pulmonary function tests including forced expiratory volume in 1 s were similar in normocapnic and hypercapnic patients (Table 1). The total specific airway resistance (sR_{tot}), respiratory resistance at 5 and 20 Hz (R5 and R20, total and proximal resistance, respectively), and R5-R20 (peripheral airway resistance) were higher in hypercapnic patients in comparison with normocapnic patients at the time of the baseline evaluation (Fig. 7, A and B). In the cohort study #2, the high respiratory resistance was improved in six patients with hypercapnia (Fig. 7C). Two of six patients had reduced hypercapnia during the course of medication, and the other four patients were on noninvasive positive pressure ventilation (NPPV) treatment for 1 week. The patients treated with NPPV did not have any history of exacerbation before the treatment nor additional medication during the treatment. We found same signaling pathways activated in mouse ASM cells when exposed to similar pCO_2 values to the COPD patients, but it took longer exposure times (fig. S9).

DISCUSSION

Here, we provide evidence of a biological pathway for airway constriction during hypercapnia. We combined unbiased molecular approaches with studies in cell culture systems and mice to show that hypercapnia promoted ASM contractility via an increase in intracellular Ca^{2+}, thereby activating Calpain-1 to cleave Caspase-7. We identify an unexpected role of Caspase-7 in ASM cells. Our results suggest that high CO_2 increases contractility via nonapoptotic activation of Caspase-7, which, by cleaving the transcription factor Mef2D, inhibits miR-133a, leading to RhoA-mediated Mlc phosphorylation.

Our findings indicate that alterations in Ca^{2+} sensitivity in ASM cells act as a primary signal by which exposure to hypercapnia enhances ASM contraction and airway hyperresponsiveness. These findings are consistent with the known effects of RhoA-mediated Ca^{2+} sensitization in regulating ASM contractility (12) and support previous data, suggesting a key role of MEF2 proteins in miR-133a regulation (23, 24). MEF2 proteins (MEF2A, MEF2B, MEF2C, and MEF2D isoforms) are an evolutionarily conserved family of transcription factors expressed in cells of many tissues including smooth muscle (25). Silencing of *Mef2c* and *Mef2d* decreased miR-133a expression levels in brown preadipocytes (24), and muscle-specific enhancers encompassing MEF2 binding sites have been identified in cardiac and skeletal muscle lineage (23). Studies have linked caspase-mediated protein fragmentation of MEF2 to its function (15, 26). It has been reported that caspase-7 cleaves MEF2D at the aspartate residue 288 in the transactivation domain, and data suggest that the remaining N-terminal cleavage products containing the DNA binding domain act as dominant-interfering forms for transcriptional regulation (15). We found that high CO_2-activated Caspase-7 cleaved Mef2D at a different aspartate residue 478 in the transactivation domain and then fragmented the protein. We observed that high CO_2 did not cause apoptosis in mouse ASM cells despite the Caspase-7 activation. Nonapoptotic functions of caspase-7 have been recently reported (27). Our data suggest that high CO_2 induces cleavage and nuclear translocation of Caspase-7 by calpain and that the calpain-truncated Caspase-7 cleaves Mef2D. The calpain-activated form of caspase-7 has been reported to have unique enzymatic activity, localization, and binding affinity in comparison with the caspase-activated form (17). The role of calpains in apoptosis has been suggested by previous studies (16); however, our data suggest that high CO_2 exposure does not induce apoptosis in mouse ASM cells and lungs, as indicated by the lack of DNA fragmentation and TUNEL-positive cells.

We found that hypercapnia increased ACh-induced ASM contraction in WT mice, which was prevented in Caspase-7-null mice. *Caspase-7* gene deletion prevented hypercapnia-induced ASM contractility by inhibiting the downstream signaling involving Mef2D, miR-133a, RhoA, and consequent Mlc phosphorylation. ASM contractility and Mlc phosphorylation are associated with intracellular Ca^{2+} concentration; however, our data show that high CO_2 causes an increase in intracellular Ca^{2+} without increasing Mlc phosphorylation in Caspase-7-null ASM cells. These findings suggest that cells regulate their intracellular Ca^{2+} concentration in discrete domains to activate specific and localized signaling pathways (compartmentalized calcium signaling) (28, 29). We speculate that hypercapnia uniquely enhances ASM contractility through a specific pool of intracellular

Ca^{2+}, which regulates the signaling pathway involving Caspase-7, Mef2D, miR-133a, and RhoA.

There are some limitations in this study. One limitation is that the magnitude of hypercapnia differs between the experiments in our in vitro system (~120 mmHg), mice (~75 mmHg), and COPD patients (45 to 88 mmHg). However, the effects are consistent with our hypothesis. Our data provide evidence on the signaling pathways activated in mouse ASM cells when exposed to pCO_2 values (~55 mmHg) similar to the observed COPD patients. Another limitation is the number of COPD patients in this report. Larger patient cohorts are warranted to provide further clinical validation to this study.

Permissive hypercapnia has been proposed to be innocuous or protective and is an accepted approach for mechanically ventilated patients with acute respiratory distress syndrome worldwide (30, 31). Whether hypercapnia should be allowed in patients with COPD is controversial. Our data are in line with recent reports that patients with COPD who develop hypercapnia benefit from noninvasive ventilation (10, 11). We show that the institution of noninvasive ventilation in hypercapnic patients with COPD improved respiratory resistance in a small group of patients. Furthermore, our in vitro data may suggest a biologically plausible mechanism to explain these benefits. These studies offer a biological mechanism that supports further studies on the effects of noninvasive ventilation on lung function in patients with COPD and also challenge the clinically accepted paradigm that hypercapnia is innocuous or beneficial in patients with COPD.

MATERIALS AND METHODS

Study design

This study was designed to determine whether hypercapnia activates signaling pathways in the airways and results in clinically significant changes in lung function. This objective was addressed by (i) an unbiased approach to understanding the role of hypercapnia in the lung by performing microarray analysis, (ii) describing the mechanism by which hypercapnia regulates ASM function in vitro, and (iii) determining whether in vitro observations translate to lung function in vivo (animal and human).

Sample sizes were estimated on the basis of pilot experiments, from previous experience in our laboratory and those reported in the literature. No data were excluded except for experiments involving administration of lentivirus particles for miR inhibitor in mice model. Exclusion criteria were preestablished. Individual samples may have been excluded on the basis of sample processing error during experimental workflow. Statistical outliers were detected and removed on the basis of Grubbs' test criteria when appropriate. All animal experiments underwent randomization at entry. Age- and gender-matched mice were randomly allocated to each experimental arm. All mice were cared for equally in an unbiased fashion by animal technicians and investigators. For the COPD cohort study, chronic stable COPD patients with or without hypercapnia, matched for age and disease severity, were recruited. Investigators were not blinded to group allocation during data correction and analysis. All in vitro and in vivo results are representative of three to seven independent experiments.

Reagents

All cell culture reagents were purchased from Corning Life Sciences. Antibodies against β-tubulin, Yy1, and RhoA were purchased from Santa Cruz Biotechnology. Antibodies against Mlc; phospho-Mlc (Ser19); total Caspase-7 and Caspase-9; cleaved Caspase-3, Caspase-7, Caspase-8, and Caspase-9; cleaved PARP; Calpain-1; Calpain-2; and H3 histone were purchased from Cell Signaling Technology. Anti-Mef2D antibody was purchased from BD Biosciences. Horseradish peroxidase (HRP)-conjugated goat anti-mouse secondary antibody was purchased from Bio-Rad, and HRP-conjugated goat anti-rabbit antibody was purchased from Cell Signaling Technology. Anti-α smooth muscle actin (α-SMA) antibody was purchased from R&D Systems. All chemicals were purchased from Sigma-Aldrich. Reagents for quantitative polymerase chain reaction (qPCR) were purchased from Life Technologies. The mRNA Isolation Kit was purchased from QIAGEN.

Cells lines and culture

Mouse ASM cell isolation and culture were performed as described elsewhere (32). Briefly, the trachea from C57BL/6J or B6.129S6-*Casp7*^{tm1Flv}/J (Caspase-7$^{-/-}$) mice was removed and transferred into Dulbecco's modified Eagle's medium (DMEM), supplemented with 10% fetal bovine serum (FBS), penicillin (100 U/ml), and streptomycin (100 μg/ml; culture medium). Connective tissue and airway epithelium were removed by firmly scraping the luminal surface. The trachea strips were cut into small pieces (~1 mm^3) and cultured in culture medium at 37°C in 5% CO_2. ASM cells begin to migrate out of the fragments after 7 to 10 days. The cells were dissociated with 0.05% trypsin and subcultured in culture medium. Identification of mouse ASM cells was based on the morphology and expression of α-SMA. Mouse ASM cells of passage <6 were used in all the experiments. Human ASM cells were obtained from Lonza and grown in culture medium.

CO_2 medium and CO_2 exposure

For the different experimental conditions, initial solutions were prepared with DMEM/Ham's F-12 medium/tris base/Mops base (3:1:0.25:0.25) containing 10% FBS, penicillin (100 U/ml), and streptomycin (100 μg/ml), as described elsewhere (6). The buffering capacity of the medium was modified by changing its initial pH with tris and Mops base to obtain a pH of 7.4 at the various CO_2 concentrations (pCO_2 of 5, 7.5, 10, and 20% for 30 to 40, 50 to 55, 60 to 80, and ~120 mmHg, respectively). In some experiments modeling extracellular acidosis, an initial pH of 6.8 was used, resulting in a final pH of 7.2 and a pCO_2 of 40 mmHg. The desired CO_2 and pH values were achieved by equilibrating the medium overnight in a humidified chamber (C-Chamber, BioSpherix). The atmosphere of the C-Chamber was controlled with a PRO CO_2 carbon dioxide controller (BioSpherix). In this chamber, cells were exposed to the desired pCO_2 while maintaining 21% O_2 balanced with N_2. Before and after CO_2 exposure, pH, pCO_2, and pO_2 values in the medium were measured using a Stat Profile pHOx blood gas analyzer (Nova Biomedical). Experiments were started by replacing the culture medium with the CO_2-equilibrated medium and incubating in the C-Chamber for the desired time.

Transfection of antagomiR-133a and mimic miR-133a

Mouse ASM cells were plated at a density of 2.0×10^5 cells per well in six-well plates with DMEM containing 10% FBS without any antibiotics. The next day, cells were transfected with 100 pmol of antagomiR-133a (AM10413, Thermo Fisher Scientific) or mimic miR-133a (PM10413, Thermo Fisher Scientific) using Lipofectamine RNAiMAX (Invitrogen), according to the manufacturer's instructions. A control precursor (AM17110, Thermo Fisher Scientific) was used as a negative control. After 5 hours in serum-free DMEM, DMEM containing 10% FBS without any antibiotics was added for 24 hours and then changed to CO_2 medium. Seventy-two hours after the transfection, cells were harvested, and total protein and RNA samples were prepared as described above.

Infection of lentiviral vector expressing miR-133

To generate cells lines of ASM cells, stably expressing miR-133, the vesicular stomatitis virus glycoprotein (VSVG)-pseudotyped lentivirus expressing both miR-133 and green fluorescent protein (GFP) was generated as described elsewhere (33) [DNA/RNA Delivery Core, Skin Disease Research Center (SDRC), Northwestern University] using 293T packaging cells (GeneHunter), second-generation packaging vectors psPAX2 and pMD2.G (Addgene), and third-generation lentiviral miR expression vector MmiR3445-MR03 (GeneCopoeia). A nonactive miR-expressing virus was used a control (CmiR0001-MR03, GeneCopoeia). Because lentiviral infection efficacy was >90%, bulk cell populations, but not individual stably infected cell clones, were used to establish the stable cell lines expressing specific or nonsilencing small hairpin RNAs.

Transfection of siRNAs

Mouse ASM cells were plated at a density of 1.1×10^5 cells per well in six-well plates with DMEM containing 10% FBS without any antibiotics. The next day, the cells were transfected with 25 nM siRNAs (siGENOME SMARTpool-*Yy1*, SMARTpool-*Mef2d*, SMARTpool-*Casp7*, SMARTpool-*Calp1*, or SMARTpool-*Calp2*, Dharmacon) using the DharmaFECT 1 Transfection Reagent (Dharmacon), according to the manufacturer's instructions. A siGENOME nontargeting siRNA pool 1 (Dharmacon) was used as a negative control. At 24 hours after transfection, the cells were cultured in the CO_2 medium. At 72 hours after transfection, cells were harvested, and total RNA or protein samples were prepared as described above.

MEF2D mutagenesis and generation of stable cell lines

Site-directed mutagenesis was used to identify and evaluate Caspase-7 cleavage of Mef2D. Point mutations (Asp to Ala, DXXD to DXXA) were introduced into a pMef2D-3XFlag (Addgene) expression vector by the QuikChange II XL Site-Directed Mutagenesis Kit (Agilent Technologies), as recommended by the manufacturer with primers containing the desired mutations as follows: *D105A*, CTGCTCCAGTGAGGCCTCCCCATCCGG (forward) and CCGGATGGGGAGGCCTCACTGGAGCAG (reverse); *D291A*, GCTGGGCATTGTTCAGAGCTAAATGGTCCTCAGTC (forward) and GACTGAGGACCATTT AGCTCTGAACAATGCCCAGC (reverse); *D478A*, CCCCCCGTCCAGCATCCCGGTCC (forward) and

GGACCGGGATGCTGGACGGGGGG (reverse). The mutations were confirmed by DNA sequencing (NUSeq Core Facility, Center for Genetic Medicine, Northwestern University). The DXXA Mef2D mutant and WT Mef2D were cloned into a third-generation lentiviral vector (CD510B, System Biosciences). Mouse ASM cell lines stably expressing DXXA Mef2D and WT Mef2D were generated by infection with the third-generation VSVG-pseudotyped lentivirus. The lentiviruses were produced and used as described above (33).

Measurement of cell contraction

Cell contraction was assessed according to the technique described elsewhere (34). ASM cells were sparsely plated onto 40-mm glass coverslips and cultured under different CO_2 conditions for the desired time. In some experiments, cells were treated with Y-27632 (final concentration, 1 μM) or infected with lentivirus expressing both miR-133 and GFP during the culture. The coverslip was mounted in an environmental control system chamber, and images were taken using a Nikon TE2000U microscope (Nikon Instruments) equipped with a digital camera driven by MetaMorph software (Molecular Devices). An initial recording (time, 0 min) was made to obtain the size of quiescent cells. Experiments were started by replacing the culture medium with the CO_2-equilibrated medium and incubating in the environmental control system chamber for the specified time. For the agonist-induced contraction experiment, ACh was added to the chamber, and images were recorded at 10-s intervals for 5 min. Cell contraction was calculated as the ratio of the change in surface area to the initial value using ImageJ (National Institutes of Health). In our preliminary experiments using mouse ASM cells under normocapnic conditions, ACh-induced cell contraction was induced in a dose-dependent manner. On the basis of this result, we chose 1 μM ACh, which is the lowest concentration to induce cell contraction, for subsequent experiments. In the experiments using cells infected with lentivirus expressing miR-133, we specifically analyzed the cells having GFP fluorescence.

Cell lysate and Western blot analysis

Cells were homogenized in lysis buffer (Cell Signaling Technology). Lung samples were homogenized on ice with cold lysis buffer in a 10-fold (w/w) excess of lysis buffer with pH of 7.6 (Roche) using a Polytron PT 10–35 homogenizer (Thermo Fisher Scientific). The protein concentration was quantified by the Bradford assay (Bio-Rad), and proteins were resolved on 7.5 or 12.5% polyacrylamide gels. Thereafter, proteins were transferred to nitrocellulose membranes (Bio-Rad) using a Trans-Blot Turbo transfer system (Bio-Rad). Incubation with specific antibodies was performed overnight at 4°C. Blots were developed with a chemiluminescence detection kit (PerkinElmer Life Sciences), as recommended by the manufacturer. The bands were quantified by densitometric scanning (ImageJ). Anti-β-tubulin (Santa Cruz Biotechnology) and total Mlc (Cell Signaling Technology) antibodies were used as loading controls.

Quantitative reverse transcription PCR

To isolate total RNA from lungs, left main bronchial rings and cells were homogenized directly in 700 μl of lysis/binding buffer provided by the miRNeasy Mini Kit (QIAGEN). Total RNA was transcribed into complementary DNA (cDNA) using a TaqMan microRNA reverse transcription kit (Life Technologies), and qPCR was performed using cDNA with

TaqMan Universal Master Mix II (Life Technologies), according to the manufacturer's instructions. The assay numbers for endogenous control miR [U6 snRNA (small nuclear RNA)] and target miR (hsa-miR-133a) were 1973 and 2246, respectively. cDNA was generated using a T100 thermal cycler (Bio-Rad), and reverse transcription PCR was performed using an iCycler iQ system (Bio-Rad). Relative expression of the transcripts was determined according to the $\Delta\Delta C_t$ method using U6 snRNA as reference for normalization.

Immunocytochemistry

Mouse ASM cells were fixed in 3.7% formaldehyde and permeabilized with 0.5% Triton X-100 in phosphate-buffered saline (PBS) for 5 min. Cells were blocked with 10% normal goat serum in PBS for 1 hour at room temperature and incubated overnight at 4°C with primary antibody Mef2D (1:500; BD Biosciences) in 10% normal goat serum. Cells were washed three times with PBS for 10 min and incubated with secondary antibodies conjugated to fluorescein isothiocyanate (1:200; Invitrogen) in 10% normal goat serum for 2 hours at room temperature. Cells were washed three times with PBS and stained with DAPI (Sigma-Aldrich) for 15 min at room temperature. Cells were washed three times with PBS, and images were captured using a Zeiss LSM confocal microscope (Carl Zeiss).

Nuclear and cytosol fractions

ASM cells were harvested, and then, nuclear/cytosol fractionation was performed with a commercially available kit (BioVision), according to the manufacturer's instructions. The nuclear/cytosol fraction was then sampled, and proteins were separated by SDS-polyacrylamide gel electrophoresis, transferred to nitrocellulose membranes, and immunoblotted with anti-Mef2D antibody (BD Biosciences) and anti-cleaved Caspase-7 antibody (Cell Signaling Technology). Anti-H3 histone antibody (Cell Signaling Technology) was used as loading controls for nuclear fractions.

Chromatin immunoprecipitation

Native protein-DNA complexes were cross-linked by treatment with 1% formaldehyde for 15 min. A SimpleChIP Plus Enzymatic Chromatin IP kit (Cell Signaling Technology) was used according to the manufacturer's protocol. Briefly, equal aliquots of isolated chromatin were subjected to immunoprecipitation with anti-Mef2D antibody (Santa Cruz Biotechnology) or mouse immunoglobulin G control (Active Motif). PCR reactions of immunoprecipitated DNA were performed to validate Mef2D binding on the miR-133a promoter. The following PCR primers were designed on the basis of the computational prediction analysis of transcription factor binding sites using TRANSFAC (www.gene-regulation.com/pub/databases.html): (#1) GGGAGAATCTGGGAAATGTA (forward) and AAAGCTGAGGAGGATTCTAT (reverse); (#2) AGCAAGATAGAATCCTCCTCA (forward) and AGGCAGCTAAGCATTTGAAACA (reverse). The PCR products were separated by gel electrophoresis.

Measurement of calpain activity

Calpain activity in total cell lysates was determined using a calpain activity assay kit (BioVision), according to the manufacturer's instructions. Briefly, mouse ASM cells were

collected and lysed in extraction buffer. Equal amounts of protein were added to the calpain substrate Ac-LLY-AFC. Fluorescence intensity indicating calpain activity was measured at 400-nm excitation and 505-nm emission wavelengths using a microplate reader (SpectraMax Microplate Reader, Molecular Devices).

Measurement of intracellular calcium

Cells plated on 40-mm coverslips were loaded with fura-2-acetoxymethyl ester (Fura-2-AM; Life Technologies) with 0.05% Pluronic F-127 (Life Technologies) and 2.5 mM probenecid (Sigma-Aldrich) for 30 min at room temperature in standard buffer solution [150 mM NaCl, 5 mM KCl, 1 mM $MgCl_2$, 10 mM glucose, 25 mM sodium bicarbonate, and 2.5 mM $CaCl_2$ (pH 7.4)] in the dark, washed with PBS, and further incubated for 30 min at room temperature to complete deesterification of the dye. Fura-2 dye was excited through 340-nm and 380-nm interference filters housed in a computer-controlled wheel. The fluorescence emitted was collected at 510 nm. The data acquisition of Fura-2 video imaging was obtained using a Nikon TE2000U (Nikon Instruments) equipped with an environmental control system chamber (FCS2 System, Bioptechs) and a Plan Super Fluor 40× oil objective (Nikon Instruments). Images were collected with a cascade electron-multiplying charge-coupled device camera TC285 with on-chip multiplication gain (Photometrics) driven by MetaFluor software (Molecular Devices). Changes in calcium concentration were obtained from the F_{340}/F_{380} ratio.

Animals

Adult (9 to 11 weeks old) male and female C57BL/6J mice and Caspase-$7^{-/-}$ mice, which are on the C57BL/6J genetic background, were obtained from the Jackson Laboratories. All animals were provided with food and water ad libitum, maintained on a 14-hour light/10-hour dark cycle, and handled according to National Institutes of Health guidelines. All of the procedures involving animals were approved by the Northwestern University Institutional Animal Care and Use Committee (IS00000245). For high CO_2 exposure, animals were maintained in a BioSpherix C-Shuttle Glove Box (BioSpherix) for 3, 7, or 21 days. The chamber's atmosphere was continuously monitored and adjusted with ProOx/ProCO_2 controllers (BioSpherix) to maintain 10% CO_2 and 21% O2, with a temperature of 23° to 26°C and a relative humidity between 30 and 50%. These settings resulted in $PaCO_2$ of ~75 mmHg and $PaCO_2$ of ~100 mmHg, whereas, in animals maintained in room air, $PaCO_2$ was ~40 mmHg and $PaCO_2$ was ~100 mmHg (35). None of the animals developed appreciable distress. Some mice were infected by intratracheal administration (36) of the lentivirus particles for miR inhibitor-scrambled control (LPP-CmiR-AN0001-AM04–100-C) or antagomiR-133a (LPP-MmR-AN0166-AM04–200) from Genecopoeia before high CO_2 exposure. At selected time points, animals were euthanized with Euthasol (pentobarbital sodium-phenytoin sodium), and trachea, whole lung, or an ~3-mm length of left main bronchial ring (14) was excised. Then, either cell was isolated or tissue was snap-frozen in liquid nitrogen for protein or RNA extraction.

Measurement of airway contraction

The lungs were excised for PCLSs. Each PCLS was prepared as described elsewhere (37). After tracheotomy, excised mouse lungs were insufflated with 2.5% low melting point

agarose in PBS. The insufflated lungs were then placed in cold PBS. After the agarose gelled, the right lobe was separated and then sectioned into slices of 100-μm-thick each using a tissue slicer (VF-300, Precisionary Instruments). Lung slices were incubated at 37°C in culture medium. The medium was changed once per hour for 3 hours. Thereafter, the PCLSs were exposed to 1 μM ACh for 2 min. Changes in the cross-sectional area of the airway lumen were monitored with a Nikon TE2000U microscope (Nikon Instruments) equipped with a digital camera (Photometrics) driven by MetaMorph software (Molecular Devices), recorded in time-lapse mode at 1 frame per 10 s, and measured by pixel summing using ImageJ. A decrease in the cross-sectional area was considered to be airway constriction.

Measurement of airway resistance

To measure airway hyperresponsiveness, mice were sedated using sodium pentobarbital (60 mg/kg) and tracheostomized with a catheter. After successful anesthesia, mechanical ventilation was started using the flexiVent System (emka TECHNOLOGIES), according to the manufacturer's instructions. Next, the mice were paralyzed with an intraperitoneal injection of 50 ml of rocuronium (10 mg/ml). After no independent breaths were recorded, the forced oscillation protocol was begun, with nebulized exposure to doses of methacholine of 0, 5, 10, 25, and 50 mg/ml in PBS. A coefficient of determination of 0.95 was the lower limit for accepting a measurement. The mean value of each methacholine concentration was used for the analysis of resistance.

Human subjects

Patients with chronic stable COPD with or without hypercapnia, matched for age and disease severity, were recruited at Hospital del Mar between December 2014 and December 2016 (cohort study #1) and at Showa University Hospital between November 2015 and August 2017 (cohort study #2). The inclusion criteria for patients were as follows: fulfilled the spirometric criteria of the global initiative for chronic obstructive lung disease guidelines, age of ≥40 years, and current or ex-smoker with a smoking history of >10 pack-years. Subjects with asthma diagnosed clinically by respiratory physicians, but not based on any bronchodilator reversibility, at the time of study entry were excluded. The study population, sex, age, body mass index, arterial blood gas results, and lung function tests are shown in Table 1. Some patients in the cohort study #2 were treated with NPPV with inspiratory positive airway pressure (6 to 8 cmH_2O) and expiratory positive airway pressure (4 cmH_2O) for 1 week, and lung function tests were performed before and after the treatment. Those patients did not have any history of exacerbation before the treatment or additional medication during the treatment. The Ethics Committee of Hospital del Mar and of Showa University School of Medicine approved the study protocol (approval number 2013/5244/I and 2360, respectively), and written informed consent was obtained from all participants.

Plethysmography

Standard measurements including forced spirometry and body plethysmography (MasterScreen Body, JAEGER, CareFusion) according to the American Thoracic Society/

European Respiratory Society recommendations (38) were performed. The variable characterizing plethysmographic specific airways resistance was sR_{tot} (39).

IOS procedure

IOS was performed with commercial equipment (MostGraph-01, CHEST M.I.). The IOS procedure was performed according to major recommendations published by several authors (40, 41). On the day of the procedure, patients from the cohort study #2 were asked to wear a nose clip and were seated during tidal breathing with their neck slightly extended and their lips sealed tightly around the mouthpiece and while firmly supporting their cheeks with their hands. A minimum of three trials (each lasting 30 s) were performed, and mean values were taken for each value.

Statistical analysis

Statistical methods are described in the figure legends and in the relevant methods descriptions. Sample size (n) values used for statistical analyses are provided in the relevant figures. Statistical analysis was performed using GraphPad Prism (version 7.02, GraphPad Software). Normally distributed data were analyzed by parametric tests including an unpaired or paired two-tailed Student's t test for two-group comparisons or a one-way or two-way ANOVA for multiple comparisons. Variances were examined by F test or the Brown-Forsythe test. For qPCR data analysis, we performed one-sample t test against a hypothetical mean of 1 in the control group and used the Bonferroni adjustment for multiple comparisons. When groups followed a nonnormal distribution, the Mann-Whitney U test or Kruskal-Wallis test was used. Unless otherwise stated, statistical significance was calculated by an unpaired two-tailed Student's t test. P values of <0.05 were considered to be significant. All values are represented as means ± SEM or median with interquartile range. Primary data are reported in table S2.

Supplementary Material

Refer to Web version on PubMed Central for supplementary material.

Acknowledgments:

We thank L. Dada, M. Casalino-Matsuda, Y. Cheng, E. Ceco, and L. Forbes (Northwestern University) and M. Nishimura and S. Konno (Hokkaido University) for support and insightful discussions; A. Spira (Boston University) and K. V. Pandit (University of Pittsburgh School of Medicine) for assistance; K. Hirai, A. Fujiwara, and H. Sagara (Showa University School of Medicine) for help with the data from COPD patients; J. Schaffer (medical and bioscientific illustrator) for the illustration; resources provided by the Northwestern University SDRC (P30AR057216) and the NUSeq Core Facility, which is supported by the Northwestern University Center for Genetic Medicine, Feinberg School of Medicine.

Funding: This study was supported in part by the NIH (HL-085534, HL-071643, and HL-048129).

REFERENCES AND NOTES

1. Weir EK, Lòpez-Barneo J, Buckler KJ, Archer SL, Acute oxygen-sensing mechanisms. N. Engl. J. Med 353, 2042–2055 (2005). [PubMed: 16282179]
2. Haldar SM, Stamler JS, *S*-nitrosylation: Integrator of cardiovascular performance and oxygen delivery. J. Clin. Invest 123, 101–110 (2013). [PubMed: 23281416]

3. Shigemura M, Lecuona E, Sznajder JI, Effects of hypercapnia on the lung. J. Physiol 595, 2431–2437 (2017). [PubMed: 28044311]
4. Vadász I, Dada LA, Briva A, Trejo HE, Welch LC, Chen J, Tôth PT, Lecuona E, Witters LA, Schumacker PT, Chandel NS, Seeger W, Sznajder JI, AMP-activated protein kinase regulates CO_2-induced alveolar epithelial dysfunction in rats and human cells by promoting Na, K-ATPase endocytosis. J. Clin. Invest 118, 752–762 (2008). [PubMed: 18188452]
5. Oliver KM, Lenihan CR, Bruning U, Cheong A, Laffey JG, McLoughlin P, Taylor CT, Cummins EP, Hypercapnia induces cleavage and nuclear localization of RelB protein, giving insight into CO_2 sensing and signaling. J. Biol. Chem 287, 14004–14011 (2012). [PubMed: 22396550]
6. Vohwinkel CU, Lecuona E, Sun H, Sommer N, Vadâsz I, Chandel NS, Sznajder JI, Elevated CO_2 levels cause mitochondrial dysfunction and impair cell proliferation. J. Biol. Chem 286, 37067–37076 (2011). [PubMed: 21903582]
7. Connors AF Jr., Dawson NV, Thomas C, Harrell FE Jr., Desbiens N, Fulkerson WJ, Kussin P, Bellamy P, Goldman L, Knaus WA, Outcomes following acute exacerbation of severe chronic obstructive lung disease. The SUPPORT investigators (Study to Understand Prognoses and Preferences for Outcomes and Risks of Treatments). Am. J. Respir. Crit. Care Med 154, 959–967 (1996). [PubMed: 8887592]
8. Kochanek KD, Murphy SL, Xu J, Arias E, Mortality in the United States, 2013. NCHS Data Brief 2014, 1–8 (2014).
9. Wheaton AG, Cunningham TJ, Ford ES, Croft JB, Employment and activity limitations among adults with chronic obstructive pulmonary disease—United States, 2013. MMWR Morb. Mortal Wkly. Rep 64, 289–295 (2015). [PubMed: 25811677]
10. Köhnlein T, Windisch W, Köhler D, Drabik A, Geiseler J, Hartl S, Karg O, Laier-Groeneveld G, Nava S, Schönhofer B, Schucher B, Wegscheider K, Criée CP, Welte T, Non-invasive positive pressure ventilation for the treatment of severe stable chronic obstructive pulmonary disease: A prospective, multicentre, randomised, controlled clinical trial. Lancet Respir. Med 2, 698–705 (2014). [PubMed: 25066329]
11. Murphy PB, Rehal S, Arbane G, Bourke S, Calverley PMA, Crook AM, Dowson L, Duffy N, Gibson GJ, Hughes PD, Hurst JR, Lewis KE, Mukherjee R, Nickol A, Oscroft N, Patout M, Pepperell J, Smith I, Stradling JR, Wedzicha JA, Polkey MI, Elliott MW, Hart N, Effect of home noninvasive ventilation with oxygen therapy vs oxygen therapy alone on hospital readmission or death after an acute COPD exacerbation: A randomized clinical trial. JAMA 317, 2177–2186 (2017). [PubMed: 28528348]
12. Somlyo AP, Somlyo AV, Ca^{2+} sensitivity of smooth muscle and nonmuscle myosin II: Modulated by G proteins, kinases, and myosin phosphatase. Physiol. Rev 83, 1325–1358 (2003). [PubMed: 14506307]
13. Murthy KS, Signaling for contraction and relaxation in smooth muscle of the gut. Annu. Rev. Physiol 68, 345–374 (2006). [PubMed: 16460276]
14. Chiba Y, Tanabe M, Goto K, Sakai H, Misawa M, Down-regulation of miR-133a contributes to up-regulation of Rhoa in bronchial smooth muscle cells. Am. J. Respir. Crit. Care Med 180, 713–719 (2009). [PubMed: 19644046]
15. Okamoto S.-i., Li Z, Ju C, Scholzke MN, Mathews E, Cui J, Salvesen GS, Bossy-Wetzel E, Lipton SA, Dominant-interfering forms of MEF2 generated by caspase cleavage contribute to NMDA-induced neuronal apoptosis. Proc. Natl. Acad. Sci. U.S.A 99, 3974–3979 (2002). [PubMed: 11904443]
16. Orrenius S, Zhivotovsky B, Nicotera P, Regulation of cell death: The calcium-apoptosis link. Nat. Rev. Mol. Cell Biol 4, 552–565 (2003). [PubMed: 12838338]
17. Gafni J, Cong X, Chen SF, Gibson BW, Ellerby LM, Calpain-1 cleaves and activates caspase-7. J. Biol. Chem 284, 25441–25449 (2009). [PubMed: 19617626]
18. Briva A, Santos C, Malacrida L, Rocchiccioli F, Soto J, Angulo M, Batthyany C, Cairoli E, Piriz H, Adenosine triphosphate-dependent calcium signaling during ventilator-induced lung injury is amplified by hypercapnia. Exp. Lung Res 37, 471–481 (2011). [PubMed: 21870898]
19. Astin TW, Barer GR, Shaw JW, Warren PM, The action of carbon dioxide on constricted airways. J. Physiol 235, 607–623 (1973). [PubMed: 4772402]

20. Fisher HK, Hansen TA, Site of action of inhaled 6 per cent carbon dioxide in the lungs of asthmatic subjects before and after exercise. Am. Rev. Respir. Dis 114, 861–870 (1976). [PubMed: 984580]
21. Nadel JA, Widdicombe JG, Effect of changes in blood gas tensions and carotid sinus pressure on tracheal volume and total lung resistance to airflow. J. Physiol 163, 13–33 (1962). [PubMed: 14477795]
22. Iscoe S, Fisher JT, Bronchomotor responses to hypoxia and hypercapnia in decerebrate cats. J. Appl. Physiol 78, 117–123 (1995). [PubMed: 7713800]
23. Liu N, Williams AH, Kim Y, McAnally J, Bezprozvannaya S, Sutherland LB, Richardson JA, Bassel-Duby R, Olson EN, An intragenic MEF2-dependent enhancer directs muscle-specific expression of microRNAs 1 and 133. Proc. Natl. Acad. Sci. U.S.A 104, 20844–20849 (2007). [PubMed: 18093911]
24. Trajkovski M, Ahmed K, Esau CC, Stoffel M, MyomiR-133 regulates brown fat differentiation through Prdm16. Nat. Cell Biol 14, 1330–1335 (2012). [PubMed: 23143398]
25. Potthoff MJ, Olson EN, MEF2: A central regulator of diverse developmental programs. Development 134, 4131–4140 (2007). [PubMed: 17959722]
26. Li M, Linseman DA, Allen MP, Meintzer MK, Wang X, Laessig T, Wierman ME, Heidenreich KA, Myocyte enhancer factor 2A and 2D undergo phosphorylation and caspase-mediated degradation during apoptosis of rat cerebellar granule neurons. J. Neurosci 21, 6544–6552 (2001). [PubMed: 11517243]
27. Erener S, Pétrilli V, Kassner I, Minotti R, Castillo R, Santoro R, Hassa PO, Tschopp J, Hottiger MO, Inflammasome-activated caspase 7 cleaves PARP1 to enhance the expression of a subset of NF-κB target genes. Mol. Cell 46, 200–211 (2012). [PubMed: 22464733]
28. Berridge MJ, Bootman MD, Roderick HL, Calcium signalling: Dynamics, homeostasis and remodelling. Nat. Rev. Mol. Cell Biol 4, 517–529 (2003). [PubMed: 12838335]
29. Billaud M, Lohman AW, Johnstone SR, Biwer LA, Mutchler S, Isakson BE, Regulation of cellular communication by signaling microdomains in the blood vessel wall. Pharmacol. Rev 66, 513–569 (2014). [PubMed: 24671377]
30. Laffey JG, Kavanagh BP, Carbon dioxide and the critically ill—Too little of a good thing? Lancet 354, 1283–1286 (1999). [PubMed: 10520649]
31. Acute Respiratory Distress Syndrome Network, Ventilation with lower tidal volumes as compared with traditional tidal volumes for acute lung injury and the acute respiratory distress syndrome. N. Engl. J. Med 342, 1301–1308 (2000). [PubMed: 10793162]
32. Chamley-Campbell J, Campbell GR, Ross R, The smooth muscle cell in culture. Physiol. Rev 59, 1–61 (1979). [PubMed: 108688]
33. Zufferey R, Dull T, Mandel RJ, Bukovsky A, Quiroz D, Naldini L, Trono D, Self-inactivating lentivirus vector for safe and efficient in vivo gene delivery. J. Virol 72, 9873–9880 (1998). [PubMed: 9811723]
34. Jiang H, Xie Y, Abel PW, Toews ML, Townley RG, Casale TB, Tu Y, Targeting phosphoinositide 3-kinase γ in airway smooth muscle cells to suppress interleukin-13-induced mouse airway hyperresponsiveness. J. Pharmacol. Exp. Ther 342, 305–311 (2012). [PubMed: 22543031]
35. Jaitovich A, Angulo M, Lecuona E, Dada LA, Welch LC, Cheng Y, Gusarova G, Ceco E, Liu C, Shigemura M, Barreiro E, Patterson C, Nader GA, Sznajder JI, High CO2 levels cause skeletal muscle atrophy via AMP-activated kinase (AMPK), FoxO3a protein, and muscle-specific Ring finger protein 1 (MuRF1). J. Biol. Chem 290, 9183–9194 (2015). [PubMed: 25691571]
36. DuPage M, Dooley AL, Jacks T, Conditional mouse lung cancer models using adenoviral or lentiviral delivery of Cre recombinase. Nat. Protoc 4, 1064–1072 (2009). [PubMed: 19561589]
37. Bergner A, Sanderson MJ, Acetylcholine-induced calcium signaling and contraction of airway smooth muscle cells in lung slices. J. Gen. Physiol 119, 187–198 (2002). [PubMed: 11815668]
38. Pellegrino R, Viegi G, Brusasco V, Crapo RO, Burgos F, Casaburi R, Coates A, van der Grinten CPM, Gustafsson P, Hankinson J, Jensen R, Johnson DC, MacIntyre N, McKay R, Miller MR, Navajas D, Pedersen OF, Wanger J, Interpretative strategies for lung function tests. Eur. Respir. J 26, 948–968 (2005). [PubMed: 16264058]

39. Kirkby J, Stanojevic S, Welsh L, Lum S, Badier M, Beardsmore C, Custovic A, Nielsen K, Paton J, Tomalak W, Stocks J, Asthma UK, Reference equations for specific airway resistance in children: The Asthma UK initiative. Eur. Respir. J 36, 622–629 (2010). [PubMed: 20150205]

40. Oostveen E, MacLeod D, Lorino H, Farre R, Hantos Z, Desager K, Marchal F; ERS Task Force on Respiratory Impedance Measurements, The forced oscillation technique in clinical practice: Methodology, recommendations and future developments. Eur. Respir. J 22, 1026–1041 (2003). [PubMed: 14680096]

41. Bickel S, Popler J, Lesnick B, Eid N, Impulse oscillometry: Interpretation and practical applications. Chest 146, 841–847 (2014). [PubMed: 25180727]

42. Konishi K, Gibson KF, Lindell KO, Richards TJ, Zhang Y, Dhir R, Bisceglia M, Gilbert S, Yousem SA, Song JW, Kim DS, Kaminski N, Gene expression profiles of acute exacerbations of idiopathic pulmonary fibrosis. Am. J. Respir. Crit. Care Med 180, 167–175 (2009). [PubMed: 19363140]

43. Corti M, Brody AR, Harrison JH, Isolation and primary culture of murine alveolar type II cells. Am. J. Respir. Cell Mol. Biol 14, 309–315 (1996). [PubMed: 8600933]

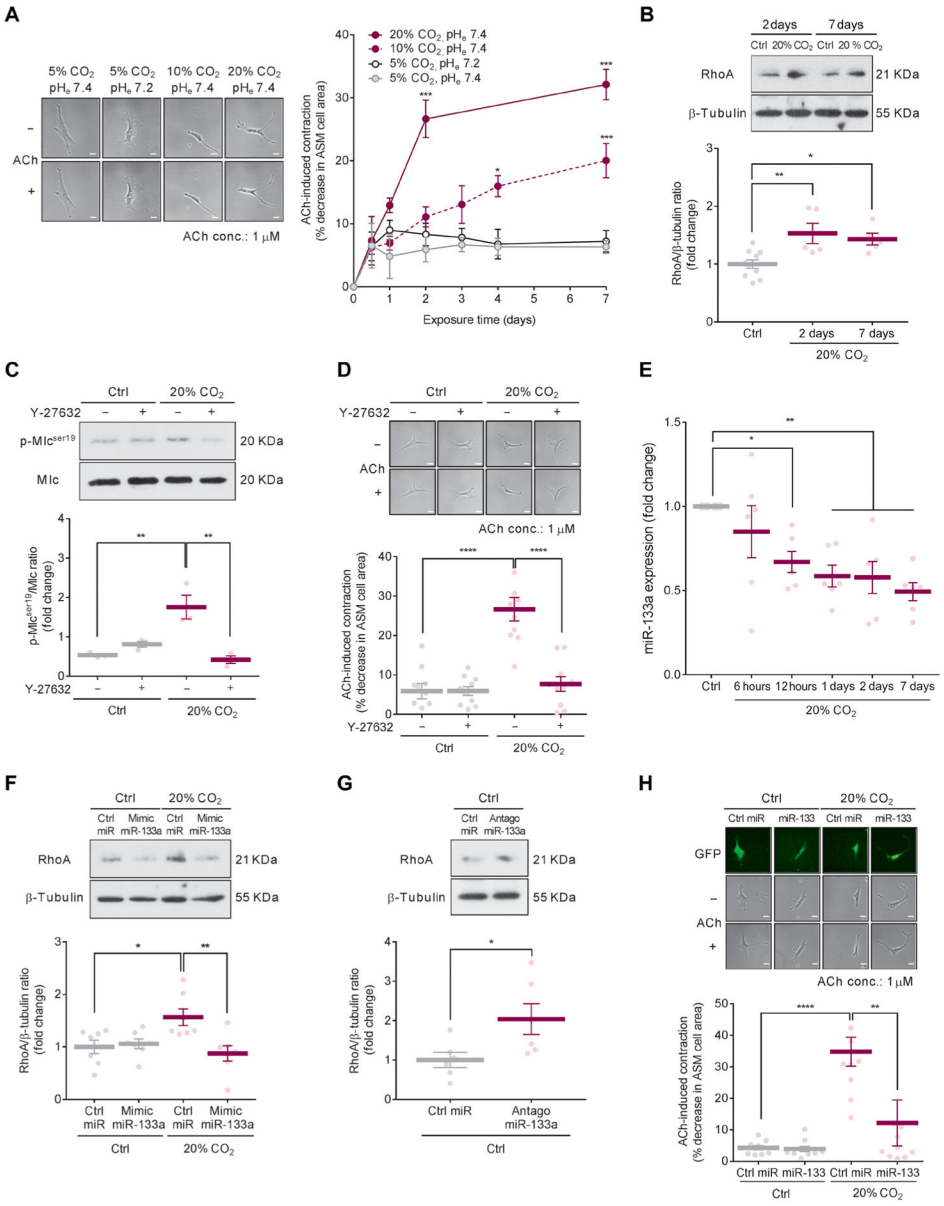

Fig. 1. High CO_2 increases mouse ASM cell contractility via miR-133a-mediated RhoA signaling.

(A) ACh-induced cell contraction in mouse ASM cells exposed to different conditions. Left: Representative images from 7-day exposure conditions. Scale bars, 50 μm. Right: Time course quantification of ACh-induced cell contraction (n = 10 cells). **(B)** Representative Western blot (top) and quantification (bottom) of RhoA in ASM cells exposed to 5% (Ctrl) or 20% CO_2 for the indicated times (Ctrl, n = 10; 20% CO_2, n = 5 per group). **(C)** Representative Western blot (top) and quantification (bottom) of phosphorylation of Mlc in ASM cells exposed to Ctrl or 20% CO_2 for 2 days in the presence or absence of 1 μM Y-27632 (n = 3). **(D)** Representative images (top) and quantification (bottom) of ACh-induced cell contraction in ASM cells exposed to Ctrl or 20% CO_2 for 2 days in the presence or absence of 1 μM Y-27632 (n = 10 cells). Scale bars, 50 μm (top). **(E)** Time course quantification of miR-133a expression in ASM cells exposed to Ctrl or 20%CO_2 (n = 6). **(F)**

Representative Western blot (top) and quantification (bottom) of RhoA in ASM cells transfected with mimic miR-133a and exposed to Ctrl or 20% CO_2 for 2 days ($n = 7$). **(G)** Representative Western blot (top) and quantification (bottom) of RhoA in ASM cells transfected with antagomiR-133a and exposed to Ctrl for 2 days ($n = 6$). **(H)** Representative images (top) and quantification (bottom) of ACh-induced cell contraction in ASM cells with lentiviral overexpression of control miR (Ctrl miR) or miR-133 exposed to Ctrl or 20% CO_2 for 2 days ($n = 10$ cells). Scale bars, 50 μm (top). All data are expressed as means ± SEM. Statistical analysis was performed by two-way analysis of variance (ANOVA) with Bonferroni's post hoc test (A), one-way ANOVA with Dunnett's post hoc test (B), Tukey's post hoc test (C, D, F, and H), or one-sample *t* test with Bonferroni adjustment (E). For (A), (B), and (E), all comparisons were made with the control group of "5% CO_2 pH_e7.4"(A) or "Ctrl" (B and E). *$P < 0.05$, **$P < 0.01$, ***$P < 0.001$, ****$p < 0.0001$.

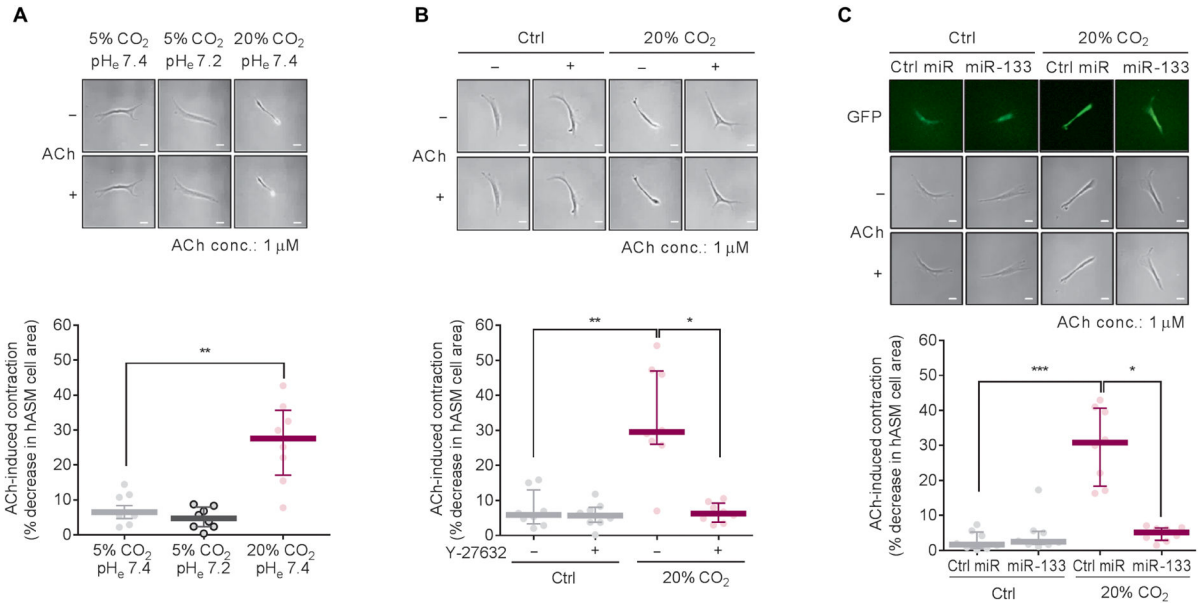

Fig. 2. High CO_2 increases ACh-induced cell contraction via miR-133a-RhoA axis signaling in human ASM cells.

All experiments were performed in human ASM (hASM) cells exposed to 5% (Ctrl) or 20% CO_2 for 2 days. **(A)** Representative images (top) and quantification (bottom) of ACh-induced cell contraction ($n = 8$ cells). Scale bars, 50 μm (top). **(B)** Representative images (top) and quantification (bottom) of ACh-induced cell contraction in human ASM cells treated with or without 1 μM Y-27632 ($n = 8$ cells). Scale bars, 50 μm (top). **(C)** Representative images (top) and quantification (bottom) of ACh-induced cell contraction in human ASM cells with lentiviral overexpression of control miR (Ctrl miR) or miR-133 ($n = 8$ cells). Scale bars, 50 μm (top). All data are expressed as median with interquartile range. Statistical analysis was performed by Kruskal-Wallis with Dunn's post hoc test. $*P < 0.05$, $**P < 0.01$, $***P < 0.001$.

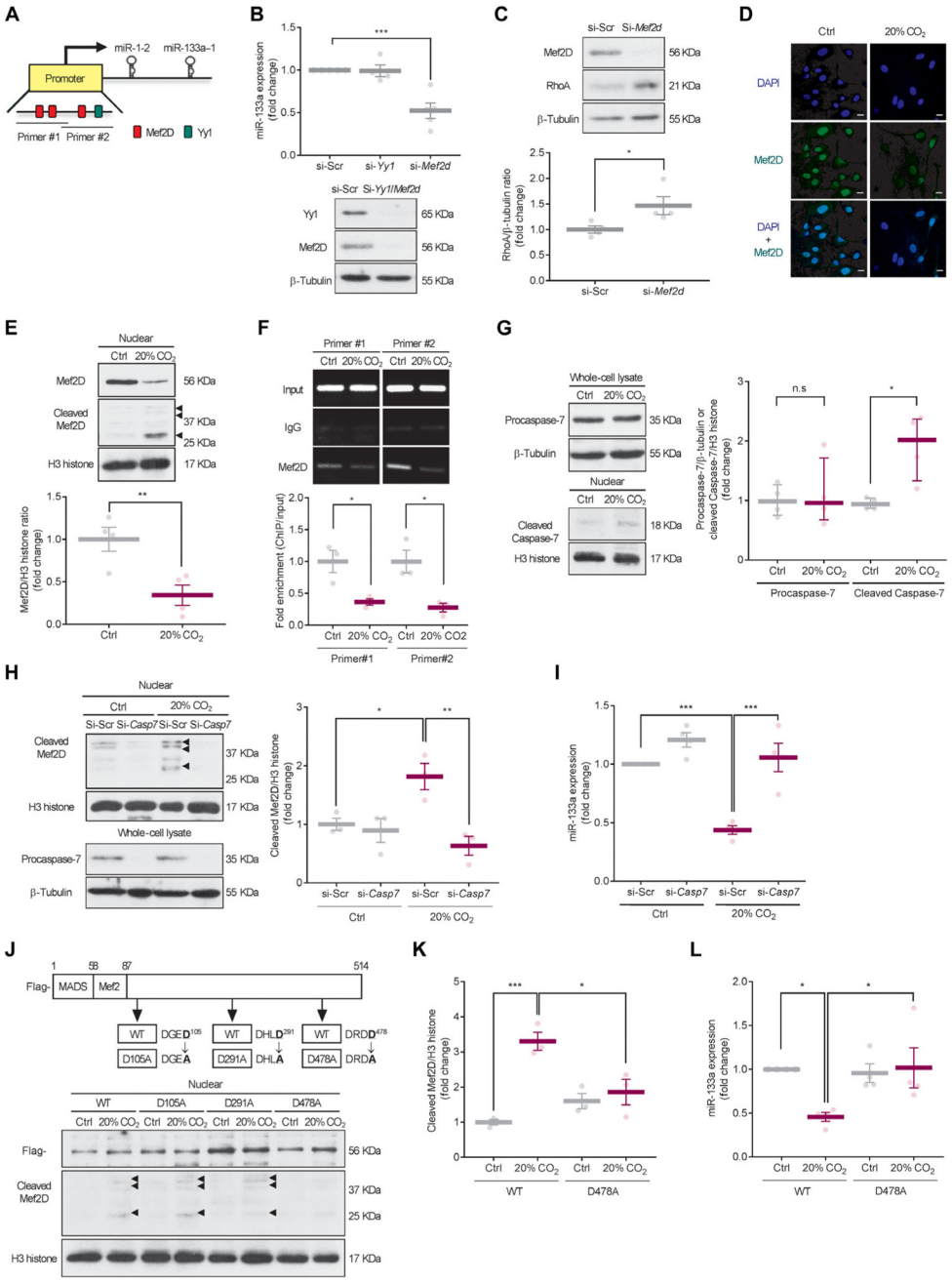

Fig. 3. High CO_2 induces Caspase-7-dependent cleavage of Mef2D and miR-133a down-regulation.

(A) Image of computational prediction analysis of transcription factor binding sites of miR-133a. Primer positions for chromatin immunoprecipitation (ChIP) assay in the promotor region of miR-133a are indicated as Primer #1 or Primer #2. **(B)** Expression of miR-133a (top) and representative Western blot (bottom) of Yy1 and Mef2D in mouse ASM cells transfected with siRNAs of scrambled (si-Scr; $n = 5$), *Yy1*(si-*Yy1*, $n = 4$), or *Mef2d* (si-*Mef2d;* $n = 5$) and exposed to 5% CO_2 (Ctrl) for 2 days. **(C)** Representative Western blot (top) and quantification (bottom) of RhoA in ASM cells transfected with si-*Mef2d* and exposed to Ctrl for 2 days ($n = 4$). **(D)** Immunocytochemical images of ASM cells exposed

to Ctrl or 20% CO_2 for 2 days showing localization of Mef2D (green; middle), nuclei [4', 6-diamidino-2-phenylindole (DAPI), blue; top], and overlay (bottom; $n > 50$ cells). Scale bars, 20 μm. **(E)** Representative Western blot (top) and quantification (bottom) of Mef2D in nuclear fractions from ASM cells exposed to Ctrl or 20% CO_2 for 2 days ($n = 4$). Arrowheads indicate cleaved Mef2D. **(F)** Representative images (top) and quantification (bottom) of ChIP assay for Mef2D binding to miR-133a promoter in ASM cells exposed to Ctrl or 20% CO_2 for 2 days using two different primer sets ($n = 3$). IgG, immunoglobulin G. **(G)** Representative Western blots (left) and quantification (right) of procaspase-7 in whole-cell lysates ($n = 4$) and cleaved Caspase-7 in nuclear fractions ($n = 4$) from ASM cells exposed to Ctrl or 20% CO_2 for 2 days. **(H)** Representative Western blot (left) and quantification (right) of cleaved Mef2D in nuclear fractions (top) and procaspase-7 in whole-cell lysates (bottom) from ASM cells transfected with si-Scr or *Caspase-7* siRNA (si-*Casp7*) and exposed to Ctrl or 20% CO_2 for 2 days ($n = 3$). Arrowheads indicate cleaved Mef2D. **(I)** Expression of miR-133a in ASM cells transfected with si-Scr or si-*Casp7* and exposed to Ctrl or 20% CO_2 for 2 days ($n = 4$). **(J)** Potential Caspase-7 cleavage sites of Mef2D (top) and representative Western blot of cleaved Mef2D (bottom) in nuclear fractions from ASM cells infected with lentiviral wild-type (WT) or mutant Mef2D and exposed to Ctrl or 20% CO_2 for 2 days ($n = 3$). Flag was used as a marker of lentiviral infection. Arrowheads indicate cleaved MEF2D. **(K** and **L)** Quantification of cleaved Mef2D (K; $n = 3$) and expression of miR-133a (L; $n = 4$) in ASM cells infected with lentiviral WT or mutant Mef2D (D478A) and exposed to Ctrl or 20% CO_2 for 2 days. Data are expressed as means ± SEM (B to F and H to L) or median with interquartile range (G). Statistical analysis was performed by one-sample *t* test with Bonferroni adjustment (B), Mann-Whitney *U* test (G), or one-way ANOVA with Dunnett's post hoc test (H to L). For (B), all comparisons were made with the control group of "si-Scr". $*P < 0.05$, $**P < 0.01$, $***P < 0.001$. n.s., nonsignificant.

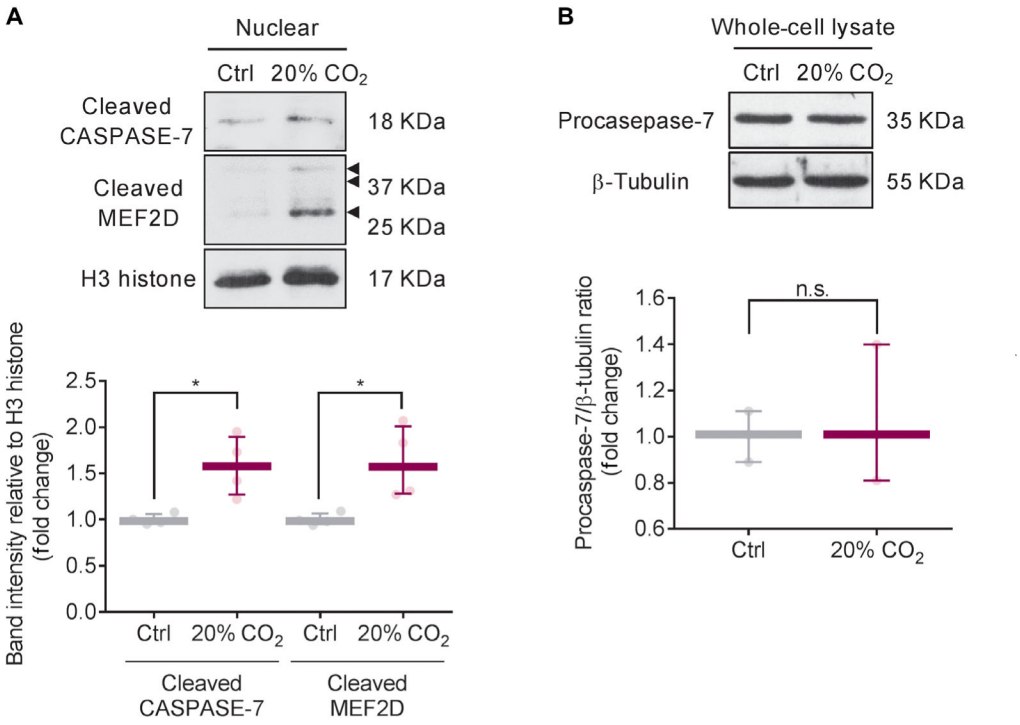

Fig. 4. High CO_2 induces CASPASE-7-dependent cleavage of MEF2D in human ASM cells.

Representative Western blot (top) and quantification (bottom) of cleaved CASPASE-7 (n = 4) and MEF2D (n = 4) in nuclear fraction **(A)** and procaspase-7 (n = 3) in whole-cell lysate **(B)** in human ASM cells. All data are expressed as median with interquartile range. Statistical analysis was performed by Mann-Whitney U test. *P < 0.05.

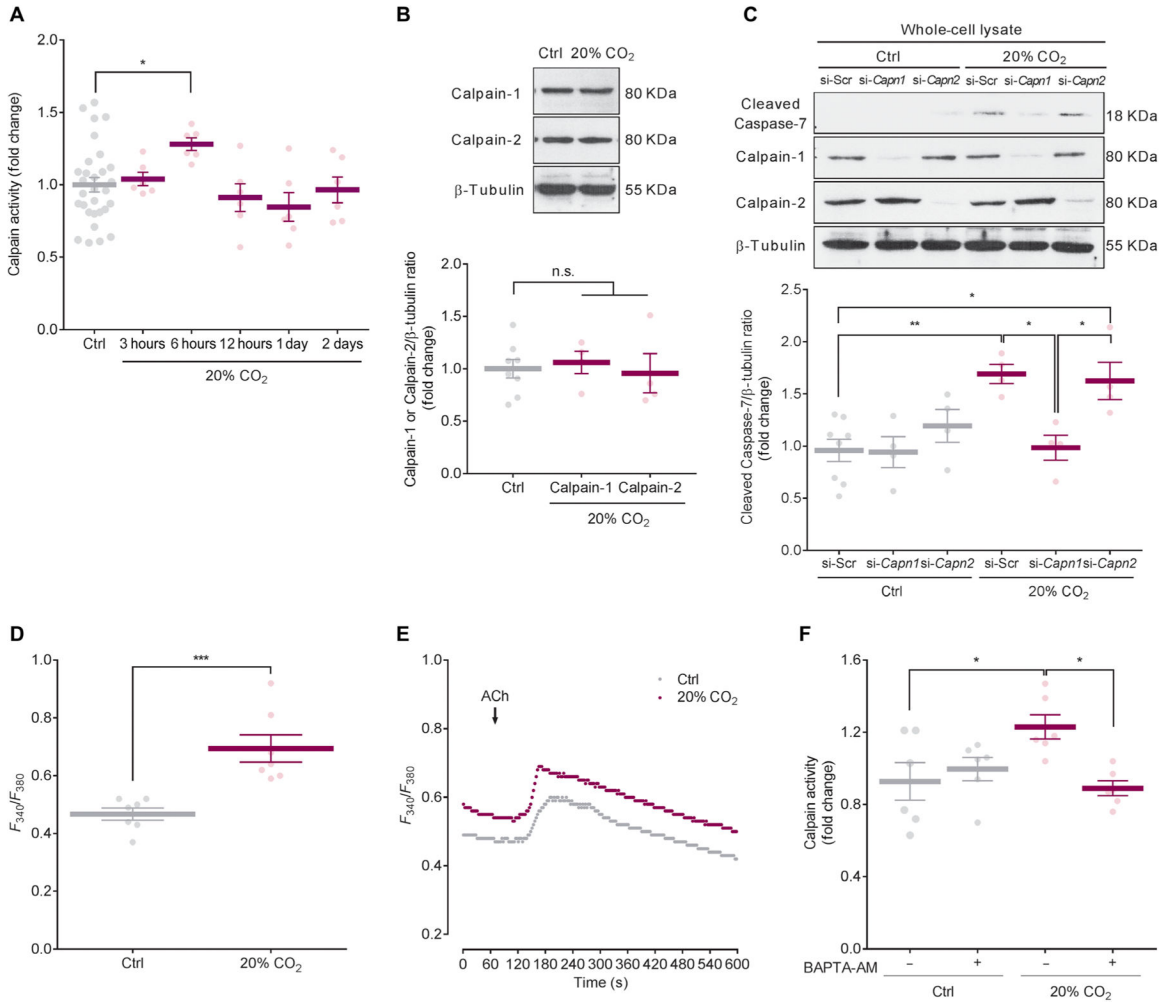

Fig. 5. High CO_2 activates calcium-calpain signaling, leading to Caspase-7 activation.

(A) Time course of calpain activity in mouse ASM cells exposed to 5% (Ctrl) or 20% CO_2 (Ctrl, $n = 30$; 20% CO_2, $n = 6$ per group). **(B)** Representative Western blot (top) and quantification (bottom) of Calpain-1 and Calpain-2 in ASM cells exposed to Ctrl or 20% CO_2 for 6 hours (Ctrl, $n = 8$; 20% CO_2, $n = 4$ per group). **(C)** Representative Western blot (top) and quantification (bottom) of cleaved Caspase-7 in ASM cells transfected with si-Scr, *Calpain-1* (si-*Capn1*), or *Calpain-2* (si-*Capn2*) and exposed to Ctrl or 20% CO_2 for 2 days (Ctrl si-Scr, $n = 8$; others, $n = 4$ per group). **(D)** Intracellular Ca^{2+} in ASM cells exposed to Ctrl or 20% CO_2 for 6 hours ($n = 7$ cells). **(E)** Representative Ca^{2+} oscillation induced by ACh in ASM cells exposed to Ctrl or 20% CO_2 for 6 hours (***n* = 7 cells). **(F)** Calpain activity in ASM cells treated with or without 1 μM BAPTA-AM and exposed to Ctrl or 20% CO_2 for 6 hours ($n = 6$). All data are expressed as means ± SEM. Statistical analysis was performed by one-way ANOVA with Dunnett's post hoc test (A and B) or with Tukey's post hoc test (C and F). For (A) and (B), all comparisons were made with the control group. $*P < 0.05$, $**P < 0.01$, $***P < 0.001$.

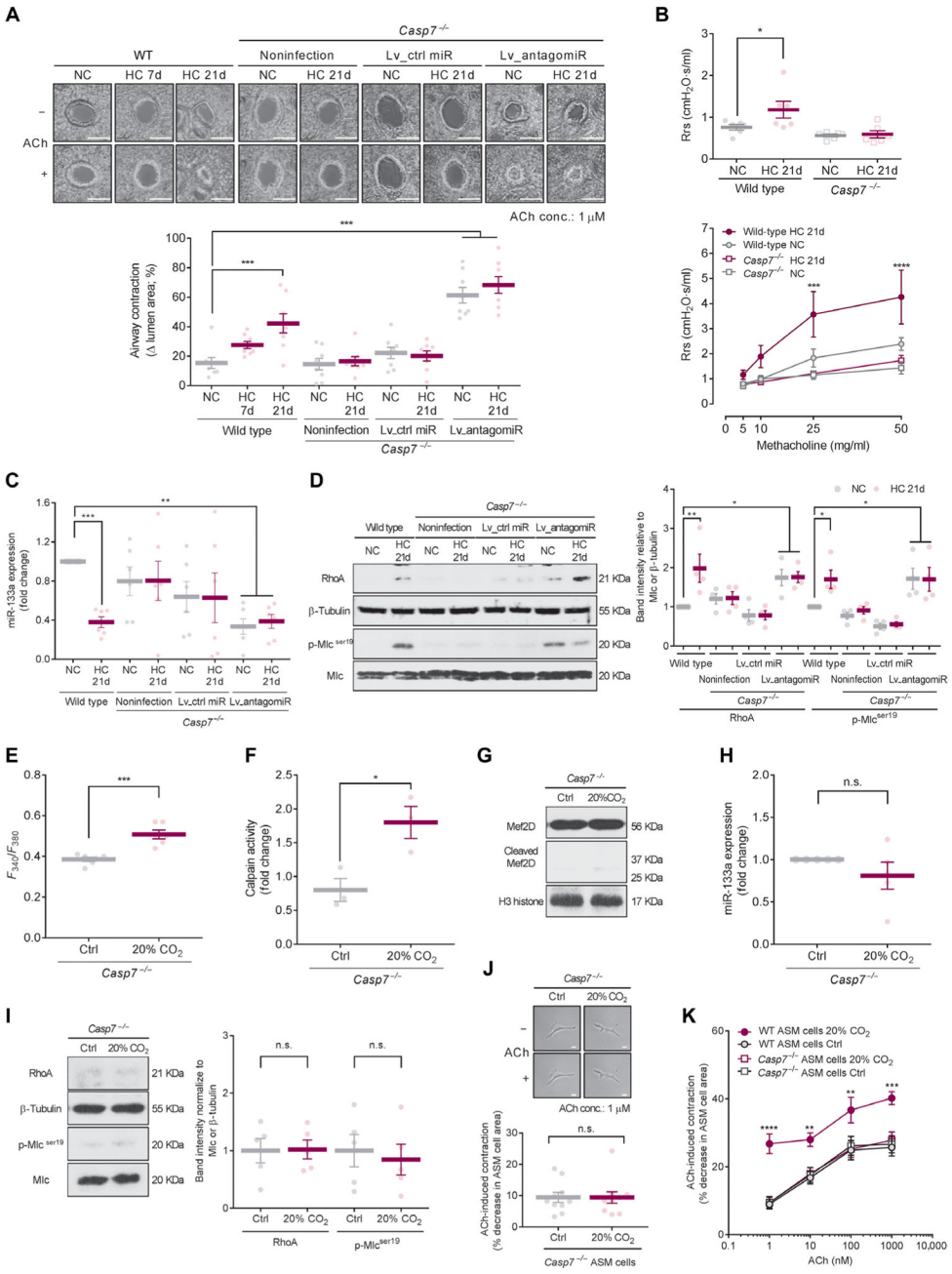

Fig. 6. Chronic hypercapnia induces airway contractility, which is prevented in Caspase-7-null mice.

C57BL/6J (WT) and B6.129S6-*Casp7*^{tm1Flv}/J (*Casp7*$^{-/-}$) mice were exposed to 21 % O_2 and 10% CO_2 [hypercapnia (HC)] or maintained in room air [normocapnia (NC)] for up to 21 days. Some *Casp7*$^{-/-}$ mice were infected by intratracheal administration of the lentivirus particles for miR inhibitor-scrambled control (Lv_ctrl miR) or antagomiR-133a (Lv_antagomiR) before HC exposure. **(A)** Representative images (top) and quantification (bottom) of ACh-induced airway contraction in PCLSs (n = 8 airways from four mice). Scale bars, 100 μm (top). **(B)** Total resistance of the respiratory system (Rrs) at baseline (top) and after methacholine challenge (bottom) measured on a flexiVent instrument (n = 6

mice). **(C)** Expression of miR-133a in left main bronchial rings (n = 6 mice). **(D)** Representative Western blot (left) and quantification (right) of RhoA and Mlc phosphorylation in whole lungs (n = 4 mice). **(E)** Intracellular Ca^{2+} in *Casp7*$^{-/-}$ ASM cells exposed to 5% (Ctrl) or 20% CO_2 for 6 hours (n = 6 cells). **(F)** Calpain activity in *Casp7*$^{-/-}$ ASM cells exposed to Ctrl or 20% CO_2 for 6 hours (n = 3). (G) Representative Western blot of Mef2D in nuclear fractions from *Casp7*$^{-/-}$ ASM cells exposed to Ctrl or 20% CO_2 for 2 days (n = 5). **(H)** Expression of miR-133a in *Casp7*$^{-/-}$ ASM cells exposed to Ctrl or 20% CO_2 for 2 days (n = 5). (I) Representative Western blot (left) and quantification (right) of RhoA and Mlc phosphorylation in *Casp7*$^{-/-}$ ASM cells exposed to Ctrl or 20% CO_2 for 2 days **(*n* =** 5). **(J)** Representative images (top) and quantification (bottom) of ACh-induced cell contraction in *Casp7*$^{-/-}$ ASM cells exposed to Ctrl or 20% CO_2 for 2 days (n = 10 cells). Scale bars, 50 μm (top). **(K)** Dose-dependent curve of ACh-induced cell contraction in WT and *Casp7*$^{-/-}$ ASM cells exposed to Ctrl or 20% CO_2 for 2 days (n = 10 cells). Data at 1 μM ACh condition in *Casp7*$^{-/-}$ ASM cells are from (J). All data are expressed as means ± SEM. Statistical analysis was performed by one-way ANOVA with Dunnett's post hoc test [A, B (top), and D (right)], one-sample t test (H), with Bonferroni adjustment (C), or two-way ANOVA with Dunnett's post hoc test [B (bottom) and K]. All comparisons were made with the group of "WT NC" (A to D) and "WT ASM cells Ctrl" (K). *P < 0.05, **P < 0.01, ***P < 0.001.

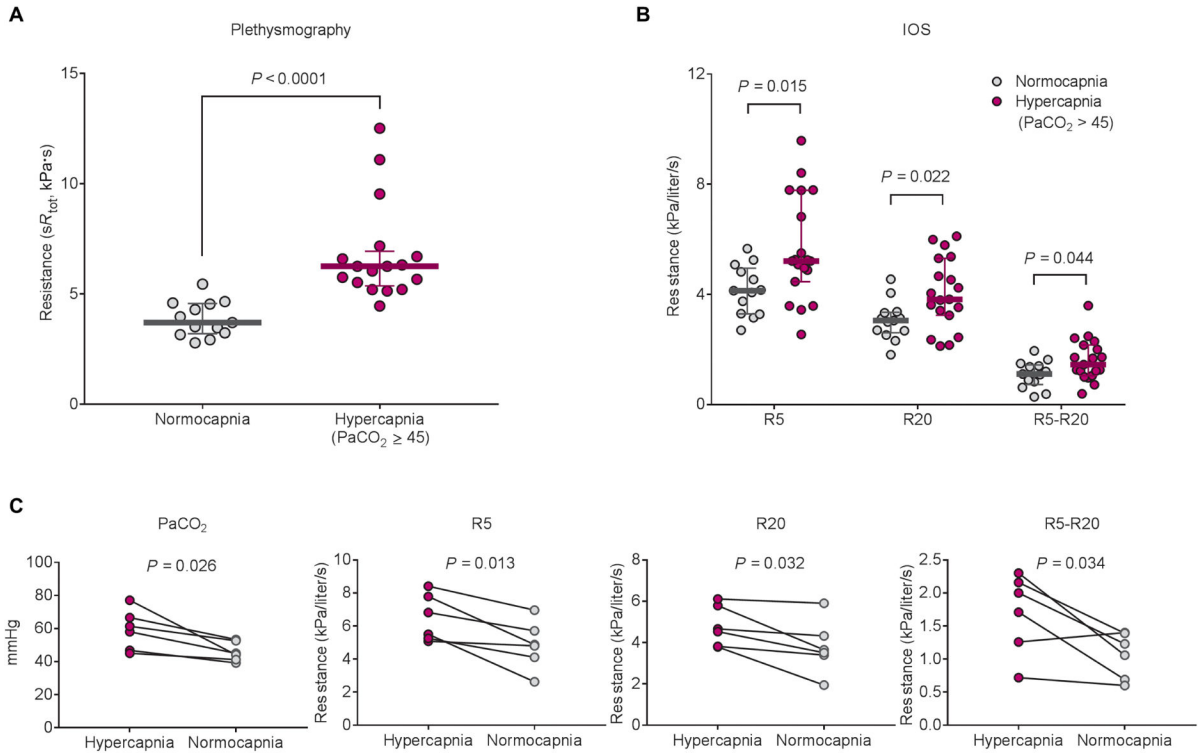

Fig. 7. Airway/respiratory resistance is increased in hypercapnic patients with COPD.

(A) Comparison of sR_{tot} measured by plethysmographic assessment between normocapnic ($n = 13$) and hypercapnic ($n = 17$) patients with chronic stable COPD in the cohort study #1. **(B)** Comparison of respiratory resistance measured by IOS between normocapnic ($n = 13$) and hypercapnic ($n = 19$) patients with chronic stable COPD in the cohort study #2. Values of R5, R20, and R5-R20 indicate total, proximal, and peripheral respiratory resistance, respectively. **(C)** Changes of respiratory resistance in hypercapnic patients from the cohort study #2 ($n = 6$). Data are expressed as median with interquartile range (A and B). Statistical analysis was performed by Mann-Whitney *U* test (A and B) or paired *t* test (C).

Table 1.
Characteristics of the study population.

Data are presented as means (range). Two-tailed unpaired *t* test except where stated otherwise. PaO_2, partial pressure of O_2 in arterial blood; $PaCO_2$, partial pressure of CO_2 in arterial blood; FVC, force vital capacity; FEV_1, forced expiratory volume in 1 s;TLC, total lung capacity.

Cohort study #1: Measurement of airway resistance

	COPD patients		
	Normocapnia	**Hypercapnia**	***P* value**
No. of subjects	13	17	
Men/women	8/5	3/14	0.013 *
Age, year	66 (50–83)	67 (58–77)	0.726
Body surface area, m^2	25 (17–31)	23 (18–27)	0.226
Blood gas results			
pH	7.42 (7.33–7.45)	7.41 (7.38–7.49)	0.702
PaO_2, mmHg	68 (58–76)	62 (49–81)	0.039
$PaCO_2$, mmHg	41 (36–44)	49 (45–55)	<0.0001
Pulmonary function results			
FVC, % predicted	63 (46–78)	59 (41–86)	0.459
FEV_1, % predicted	30 (16–37)	25 (13–36)	0.094
FEV_1/FVC	35 (21–48)	33 (22–45)	0.467
TLC, % predicted	116 (76–156)	116 (96–145)	0.938

Cohort study #2: Measurement of respiratory resistance

	COPD patients		
	Normocapnia	**Hypercapnia**	***P* value**
No. of subjects	13	19	
Men/women	10/3	11/8	0.266 *
Age, year	71 (57–81)	73 (47–91)	0.436
Body surface area, m^2	22 (17–29)	21 (14–33)	0.735
Blood gas results			
pH	7.44 (7.41–7.49)	7.40 (7.32–7.47)	0.002
PaO_2, mmHg	79 (59–113)	77 (55–103)	0.644
$PaCO_2$, mmHg	39 (32–43)	54 (45–88)	<0.0001
Pulmonary function results			
FVC, % predicted	71.4 (41.8–95.4)	61.4 (35.3–84.1)	0.106
FEV_1, % predicted	42.1 (22.8–65.5)	36.0 (13.7–72.5)	0.323
FEV_1/FVC	51.1 (20.3–82.2)	47.9 (23.0–87.8)	0.713

* χ^2 test.